Yang, H., Wang, Y., Seow, C. K., Sun, M., Si, M. and Huang, L. (2023) UWB sensor based indoor LOS/NLOS localization with support vector machine learning. IEEE Sensors Journal, (doi: 10.1109/JSEN.2022.3232479).

There may be differences between this version and the published version. You are advised to consult the publisher's version if you wish to cite from it.

https://eprints.gla.ac.uk/290426/

Deposited on: 27 January 2023

Enlighten – Research publications by members of the University of Glasgow
https://eprints.gla.ac.uk

UWB Sensor based Indoor LOS/NLOS Localization with Support Vector Machine Learning

Hongchao Yang, Yunjia Wang, Chee Kiat Seow, Meng Sun, Minghao Si, and Lu Huang

Abstract*—Ultra-wideband (UWB) sensor technology is known to achieve high-precision indoor localization accuracy in line-of-sight (LOS) environments, but its localization accuracy and stability suffer detrimentally in non-line-of-sight (NLOS) conditions. Current NLOS/LOS identification based on channel impulse response's (CIR) characteristic parameters (CCP) improves location accuracy, but most CIR-based identification approaches did not sufficiently exploit the CIR information and are environment specific. This paper derives three new CCPs and proposes a novel two-step identification/classification methodology with dynamic threshold comparison (DTC) and the fuzzy credibility-based support vector machine (FC-SVM). The proposed SVM based classification methodology leverages on the derived CCPs obtained from the waveform and its channel analysis, which are more robust to environment and obstacles dynamic. This is achieved in two-step with a coarse-grained NLOS/LOS identification with the DTC strategy followed by FC-SVM to give the fine-grained result. Finally, based on the obtained identification results, a real-time ranging error mitigation strategy is then designed to improve the ranging and localization accuracy. Extensive experimental campaigns are conducted in different LOS/NLOS scenarios to evaluate the proposed methodology. The results show that the mean LOS/NLOS identification accuracy in various testing scenarios is 93.27 %, and the LOS and NLOS recalls are 94.27 % and 92.57 %, respectively. The ranging errors in LOS(NLOS) conditions are reduced from 0.106 m(1.442 m) to 0.065 m(0.739 m), demonstrating an improvement of 38.85 %(48.74 %) with 0.041 m(0.703 m) error reduction. On the other hand, the average positioning accuracy is also reduced from 0.250 m to 0.091 m with an improvement of 63.49 %(0.159 m), which outperforms the state-of-the-art approaches of the Least-squares support vector machine (LS-SVM) and K-Nearest Neighbor (KNN) algorithms.

***Index Terms*—UWB, CIR, Fuzzy Credibility, SVM, Channel identification, Ranging mitigation, Indoor positioning.**

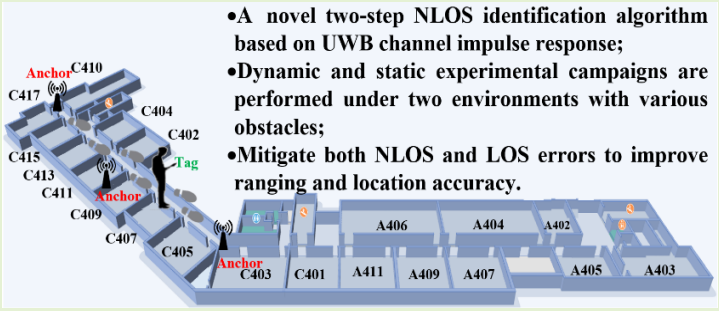

I. Introduction

LOCATION-BASED service (LBS) plays a crucial role in daily life and industrial production. In the outdoor environment, the global satellite navigation system (GNSS)[1] provides stable, high-accuracy localization services. However, the satellite signal cannot be used due to poor or no signal penetration and multipath transmission in buildings in indoor environments. This leads to poor positioning accuracy. To realize indoor localization, extensive research has been carried out on various localization technology such as Wireless Fidelity (Wi-Fi) [2], Bluetooth [3], geomagnetism [4], Ultra-wideband (UWB) [5-8], pseudo-satellite[9]. Among these approaches, UWB has attracted extensive attention due to its large transmission bandwidth that leads to high localization accuracy resolution, which can meet the requirements of indoor high-precision positioning. It has been applied to many aspects like industrial robots, unmanned aerial vehicle (UAV) search, etc. With the update of smartphone hardware, phones including Apple, Samsung, and Xiaomi have adopted UWB technology to support consumer indoor positioning applications on mobile phones such as Smart Tag, and Airtag[10].

The accuracy of the UWB hardware positioning is determined by the time-of-flight (TOF)-based ranging accuracy, which is affected by clock drift, frequency drift, received signal level, and Non-Line of Sight (NLOS) transmission [11-14]. The first three impairments are hardware related, while NLOS transmission has the direct signal propagation path between devices being blocked. NLOS [14, 15] transmission occurs frequently due to complex indoor topology and various indoor obstacles such as walls and doors. The UWB pulse signal from the transmitter must travel an extra distance to reach the receiver, resulting in a positive deviation in ranging error and hence inaccurate localization. It is necessary to first identify and suppress the NLOS signal before positioning.

Existing NLOS/LOS identification algorithms mainly comprise distance statistics-based algorithms [14-17], fusion-based technologies [18-21], and Channel Impulse Response

"This work was supported in part by the National Key Research and Development Program of China under Grant 2016YFB0502102."

Hongchao Yang, Yunjia Wang, Meng Sun, Minghao Si are with the China University of Ming and Technology and Key Laboratory of Land Environment and Disaster Monitoring, Xuzhou 221116, China, (e-mail: hongchao_yang@cumt.edu.cn;wyjc411@163.com;msun@cumt.edu.cn;hmsi@cumt.edu.cn.

Chee Kiat Seow is with the School of Computing Science, University of Glasgow, Sir Alwyn Williams Building, Glasgow G12 8RZ, Scotland, United Kingdom. (e-mail: CheeKiat.Seow@glasgow.ac.uk)

Lu Huang is with the 54th Research Institute of China Electronics Technology Group Corporation, Shijiazhuang 050081, China (e-mail: hlcetc54@163.com).

XXXX-XXXX © XXXX IEEE. Personal use is permitted, but republication/redistribution requires IEEE permission.
See http://www.ieee.org/publications_standards/publications/rights/index.html for more information.

(CIR)-based methods [22-33], which divide the data into identified-NLOS (I-NLOS) and identified LOS (I-LOS). CIR epitomizes signal fluctuation and attenuation in the channel environment. Such characteristics of different channel environments can be measured, recorded, and effectively trained with various classification algorithms for identification. Therefore, the CIR-based methodology is one of the most popular NLOS/LOS identification methodologies. Previous research works mainly focus on the distinction of the waveform and its overall energy distribution but does not reflect the key features of the waveforms. This results in poor performance robustness to dynamic environments and obstacles. Typically, the algorithms to suppress ranging errors' influence on location can be divided into two methodologies. The first methodology [34-38] is pivoted on the correction of the I-NLOS components in the dataset and combined with the I-LOS components, which can improve the position accuracy, but requires lots of complicated processing work during the correction. The second methodology [39-43] introduces additional positional information to suppress ranging error. Pedestrian Dead Reckoning (PDR) provides high relative positioning accuracy but subjects to heavy drift in the IMU components. It requires external constant calibration to correct the drift such as from UWB system. However, when the environment layout is complex, a large number of continuous NLOS measurement in the UWB system will not be able to compensate the accumulated errors of PDR and other algorithms in real time, which will reduce the stability and accuracy of the overall system. In the visual positioning system (VPS) which relies on light energy for positioning. In more complex feature texture and brightness changes, the lighting recognition and correlation to the device exact position will be in doubt and suffers inconsistency. In open and large environment, the use of Wi-Fi, BLE and vision positioning technology will reduce positioning accuracy significantly since these technologies relies heavily on feature matching as the core but the spatial change of features in large open environment is not obvious. Furthermore, existing methodologies cannot alleviate relatively high errors in LOS components in the dataset. Based on the above limitation, this paper introduces the novelty in the extraction of three new CIR characteristics parameters (CCPs) and further mines potential classification information by fuzzy credibility [44]. Combining the ranging error with the CCPs improves the mitigation algorithm with robustness in the environment dynamic. Our novel contributions are summarized as follows:

(a) We divide the whole process of the UWB hardware signal acquisition into three stages according to the fluctuation caused by the arrival of FP, namely environmental noise stage (ENS), first path signal (FP) judgement stage, and multipath (MP) stage. To the best of our knowledge, this paper is the first to introduce the UWB signal acquisition into 3 novel stages for localization/positioning. These stages are not only essential to optimize the existing CCPs but enabling the feature extraction of three new proposed CCPs namely: false crests number (FCN), FP error (FPE), and FP distance error (FDE) from the waveform and energy of key nodes. These 3 new features' parameters cover the main characteristics of the 3 proposed signal stages and classify channel environment from both time series and energy perspective in two dimensions as compared to existing CCPs which monotonously classified channel in one dimension. Hence our proposed CCPs provide much stronger feature representation and robustness in classification performance.

(b) We propose a two-step dynamic threshold comparison-fuzzy credibility-based support vector machine (DTC-FCSVM) algorithm to classify the UWB channels. Based on two proposed typical misjudgment environments, the algorithm refines the optimal CCP feature set of different pre-classification results and used the fuzzy credibility to mine potential CCPs' classification information. To ensure the performance of the first step DTC, we also update the DTC threshold (DTC-T) with the final identification result.

(c) We also design a correction strategy for the NLOS ranging error. As the ranging error is classified based on the environment noise energy fluctuation on the weakened true first path (TFP), we propose different correction schemes from the perspective of time and energy. Finally, we conduct a multi-scene experimental campaign to verify the proposed algorithms' channel identification accuracy, ranging error correction effect, and the improvement of dynamic positioning accuracy.

Section II briefly reviews the related work about UWB NLOS/LOS identification and ranging error mitigation. Section III introduces the principle of TOF-ranging and the proposed CCPs set containing three new parameters. Section IV proposes a two-step channel identification algorithm and ranging result correction strategy. In Section V, we set up the experimental campaign in multi-scenes to verify the algorithm's performance. Finally, Section VII gives some conclusions.

II. Related Works

A. LOS/NLOS Identification Algorithms

The existing identification algorithms can be divided into three categories: distance statistics-based method, fusion-based approaches, and CIR-based methods. The distance statistics-based techniques use the variance of ranging results or probability density function [14] (PDF) to distinguish the channel. Before positioning operation, the system needs to collect lots of LOS data to determine the variance threshold σ_{LOS}^2 of ranging signal, which performs well in static experiments [16]. In dynamic experiments, the threshold formula needs to introduce the known maximum velocity v_{max} to alleviate the misjudgment of LOS as NLOS due to overestimation of σ_{LOS}^2 [17]. Obviously, the algorithm can only significantly improve the recognition accuracy when the v_{max} is accurate, and it is also limited by environment constraint since the prior information of the environment needs to be repeatedly measured. Fusion-based methods need to combine other localization technologies such as inertial measurement units (IMU), visual positioning, etc. In [18], IMU is integrated with UWB and the former real-time positioning results are used to identify NLOS data through the iterative extended Kalman filter (IEKF). It does not need the prior information, but the gyro drift will affect the recognition accuracy. Research work in [20] uses the Mahalanobis distance to identify abnormal UWB ranging and control its noise covariance matrix, which is implemented on mobile phones with the low-cost IMU. However, in continuous NLOS, the performance of outlier detection based on Mahalanobis distance is influenced by walls, obstacles, and low hardware accuracy. Jo *et al.* [19] obtained the signal's statistical information from the propagation delay

XXXX-XXXX © XXXX IEEE. Personal use is permitted, but republication/redistribution requires IEEE permission.
See http://www.ieee.org/publications_standards/publications/rights/index.html for more information.

data by ray tracing and calculated the variance threshold using Cramer Rao lower bound. Its off-line training time increases exponentially with the increase of positioning area and layout complexity. In addition, the system cannot simulate all obstacles and need high-precision maps to ensure accuracy.

The CIR-based methods mainly include two steps. Firstly, CCPs are extracted from UWB sensors parameters, which are mainly divided into time and energy domains. The time-domain CCPs are based on the difference in the arrival time of the multipath signals. These mainly include rise time (t_{rise}) and the probability of NLOS (PNLOS). On the other hand, the energy CCPs are based on the signal attenuation and interference caused by obstacles. These include total energy (ε_r), standard power deviation (σ_r), mean excess delay (τ_{MED}), root mean square delay spread (τ_{rms}), kurtosis (κ), maximum amplitude CIR (r_{max}), first path power level (FPPL), receive power level (RXL), and the difference between FPPL and RXL (DFR = RXL - FPPL) and energy saturation (ES) [25]. Secondly, the channels are normally identified by combining CCPs with classification methods like threshold comparison [22], joint likelihood function [17, 23, 24], support vector machine (SVM) [25-28], and K-NN [30], etc. In [22], the mean accuracy of the single CCP threshold comparison algorithm is only 71.28 %, which does not meet the positioning requirements and has no clear threshold definition rules. Previous work [23] improves the mean accuracy from 86.9 % of single CCP to 91.3 % with joint likelihood estimation with ratio comparison of κ, τ_{MED} and τ_{rms} with the fixed threshold. The delay-spread estimate [24] of τ_{rms} can ensure classification performance when the distance is unknown, and hence improve positioning accuracy once TOF and received signal strength are further utilized. Jasurbek *et al.* [5] uses effective and dominant path number as a new CCP feature to reduce the complexity of the parameter set on the premise of ensuring accuracy. However, the recall of LOS is universally lower than the recall of NLOS. This is not conducive in the extraction for high-precision-ranging results. SVM [26] does not need much prior information and is widely used in various classification problems through pre-training models. In [27], the performance of SVM classification is compared in multiple scenarios (concrete wall, glass, wood wall) with different kernel functions, namely linear, polynomial, Gaussian, and sigmoid. Another factor is the number and composition of support vector sets to be used. Gifford *et al.* [25] discussed the impact of different CPP sets on identification accuracy and evaluated SVM's performance through Monte Carlo simulation. As the number of CPPs sets increases from 2 to 3, the identification accuracy will increase from 90 % to 91.4 %, but r_{max} has no impact to the performance once added to the set that comprise of $\{\varepsilon_r, t_{rise}, \kappa\}$. In addition, the accuracy of this set in [6] is only 89.7 %, and its optimal set contains $\{r_{max}, \tau_{MED}\}$. Kolakowski *et al.* [29] use τ_{MED} and τ_{rms} instead of DFR and ε_r to compare the accuracy of the same three-parameter sets, which can improve the recognition accuracy by 22.83 % and greatly improve the LOS recall. They also refine the classification of different NLOS namely Direct-Path NLOS when direct path component is receivable although blocked and Non-Direct-Path NLOS when direct path is completely blocked and cannot be received. However, the performance is inconsistent as it is highly site-specific. Mostly, three-parameters set is stable enough to provide high identification accuracy but optimization is needed for different scenarios to obtain the optimal effect. Qiang *et al.* [30] proposed an 8-parameter K-NN recognition algorithm with lower complexity. When the number of reference nodes are increased to 15, its accuracy is equivalent to that of the least square SVM (LS-SVM) and the offline training time is reduced by 5 seconds, but the performance shown is only for a single scenario. The identification accuracy of traditional machine learning (ML) will decrease when the types of offline data are unbalanced. Che *et al.* [31] recognized NLOS by calculating the Gaussian distribution and the generalized Gaussian distribution of energy-related features (such as FPPL and RXL), which were 3.715 % and 4.475 % more accurate than ML, respectively. Under the same parameters, the weighted Naive Bayesian algorithm [32] has better ROC curves for true and false positive rates, with an average increase of 0.17AUC area. Research work in [33] uses κ and Gabor filter to realize LOS and NLOS switching detection. However, it can only be used as an auxiliary means due to the need of accurate initial states and the error will accumulate.

In summary, the changing environment and obstacles will affect waveform identification, which leads to fluctuated classification performance using existing CCPs. In addition, the CCPs used in the existing algorithms are independently being used in the estimation, without exploring their cross-correlation to give rise to additional potential classification information. Furthermore, there is no universal CCP set that balances accuracy and robustness since it is site-specific.

B. NLOS Ranging Error Suppression Algorithm

The existing NLOS ranging error suppression algorithms are divided into two categories. The first methodology directly rectifies the ranging errors and uses the corrected range result for localization to determine the receiver's coordinates. Heidari *et al.* [34] uses τ_{rms}, FPPL and ε_r to establish the statistical error model, decreasing the root mean square (RMSE) of ranging error by 50 % to 1.56 m , but the estimation error was random. Wu *et al.* [35] iteratively estimate TFP by combining received TOF with RXL and derived NLOS ranging error expression using the signal path loss model. It can reduce the mean ranging error in the range of 2-13 m to less than 0.5 m and remain below 1m with the expansion of the positioning area. However, the correction effect in some points is detrimental due to outliers. Converting the amplitude information into rank statistics can weaken outliers' interference and effectively maximize the FP's information [36]. TFP is estimated using the row rank statistical sequence of each frame's amplitude and combines maximum likelihood to improve performance. Due to the need for ergodicity which required all signal paths, the FP evaluation algorithm is complex and time-consuming. Li *et al.* [37] use the signal means to eliminate Gaussian white noise (AWGN) and searched FP by the least square (LS) to reduce complexity. It can decrease ranging error to below 1m with 30 % to 80 % performance improvement, but it is time-consuming to process multiple signal pulses. Saeed *et al.* [38] introduce time and amplitude thresholds to improve the timeliness and reduce

XXXX-XXXX © XXXX IEEE. Personal use is permitted, but republication/redistribution requires IEEE permission.
See http://www.ieee.org/publications_standards/publications/rights/index.html for more information.

the 30 % search area. However, the selection criteria of the threshold are unclear with no comparison with existing algorithms. In general, the first methodology is time-consuming and cannot meet the real-time positioning.

The second methodology does not attempt to correct the ranging error but uses additional information and I-LOS data to solve the receiver's coordinates to suppress the NLOS ranging error. Chen *et al.* [39] estimate coordinates by integrating homologous ranging results of additional anchors and using residual weight to reduce error impact, which is relatively easy to implement. However, the average calculation time increases by 150 % when the number of nodes adds from 4 to 9. Jiao *et al.* [40] reduced average calculation time by 58.91 % under the same test condition in [39] by selecting the minimum residual combination. However, the above algorithms are required to optimize anchors' layout for different environments. Using the MSE positioning error, Zhao *et al.* [41] has developed an optimized UWB deployment scheme to balance the geometric and NLOS effects of radio locations, which reduced the two-dimensional RMSE positioning error by 47 %. Additional information can also be fused such as fusing IMU and UWB by EKF [42], which can ensure dynamic positioning continuity and reduce the standard deviation (STD) of the location to 1.14 cm. However, it requires expensive high-precision hardware to reduce the impact of the cumulative drift error by the IMU on positioning performance during continuous NLOS scenarios. On the basis of the combination of IMU and UWB, Huang *et al.* [43] proposed a positioning framework that fuses additional map information and achieved the multi-anchors positioning of hybrid LOS and NLOS by maximum likelihood estimation taking into account of clock drift error. The second methodology has low dependency on prior information and do not need error modeling but is difficult to balance add-on technology with UWB.

The above algorithms need high recognition accuracy to retain the original high-precision-ranging results and reduce the consumption of the correction algorithm. To reduce algorithms' environmental sensitivity and improve the universality, we pre-classify error according to waveform CCPs and reduce the TFP estimation's complexity by enhancing FP judgment processes.

III. Theoretical Framework

A. UWB TOF Ranging Principle

UWB TOF ranging technologies include single-sided two-way ranging (SS-TWR) and double-sided two-way ranging (DS-TWR)[45]. SS-TWR measures the signal's single round trip time on hardware timestamps (HTS) but is seriously affected by clock drift. As shown in Fig.1 DS-TWR is an extension of SS-TWR, which reduces the impact of clock drift and improves the accuracy by recording two round-trips HTS of the signal. The communication process of DS-TWR is as follows: The tag starts with sending poll frames to the anchor, HTS $poll_{tx}$ and $poll_{rx}$ are recorded by the tag and anchor respectively; after the first fixed time delay D_{round1}, the anchor sends resp frames to the tag, and the corresponding HTS is $resp_{tx}$ and $resp_{rx}$ for the anchor and tag respectively; after the second fixed time delay ($D_{round2} = Slot - T_{round1}$), the tag sends final frames to the anchor, and the corresponding HTS is $final_{tx}$ and $final_{rx}$ for the tag and anchor respectively. The TOF can be obtained as follow:

$$TOF = \frac{(T_{round1}T_{round2} - D_{round1}D_{round2})}{T_{round1} + T_{round2} + D_{round1} + D_{round2}} \quad (1)$$

where $T_{round1}, T_{round2}, D_{round1}, D_{round2}$ are calculated as:

$$\begin{aligned} T_{round1} &= resp_{rx} - poll_{tx} \\ D_{round1} &= resp_{tx} - poll_{rx} \\ D_{round2} &= final_{tx} - resp_{rx} \\ T_{round2} &= final_{rx} - resp_{tx} \end{aligned} \quad (2)$$

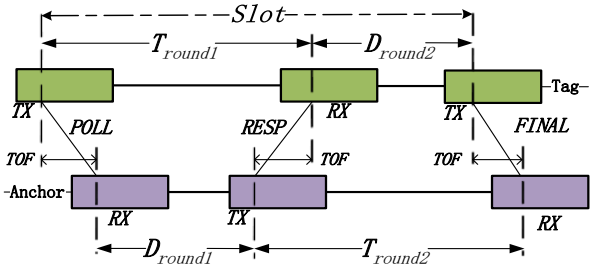

Fig. 1. Ranging process of DS-TWR. Slot represents the ranging period.

Based on TOF, the distance between the tag and anchor is calculated as:

$$distance = TOF * c \quad (3)$$

where c is the speed of light. In addition to the hardware system errors especially clock drift, ranging accuracy is mainly affected by the estimation accuracy of signal arrival time [12], that is, whether the reported first path (RFP) by the system is equivalent to TFP.

B. UWB CIR Wave Features Extraction

The communication frame reaching the receiver depends on the hardware's statistical judgment of CIR [28]. The CIR is the system's estimation of the correlation between the cumulative incoming sample and the expected lead sequence:

$$r(t) = \sum_{i=1}^{N_m} a_i p(t - \tau_i) + n(t) \quad (4)$$

where N_m is the number of multipath components; a_i and τ_i are the amplitude and delay of i^{th} component, respectively; $n(t)$ is the additive AWGN; $p(t)$ is the waveform of the UWB impulse waveform which usually is a Gaussian pulse. This paper divided the typical complete LOS/NLOS CIR communication process as shown in Fig. 2 and Fig. 3 into the environment noise stage (ENS), FP judgment stage, and multipath stage (MP).

During communication, the system dynamically calculates the FP decision threshold L (LDE-Thre) based on the leading-edge detection (LDE) algorithm [46] as shown in Fig 2. Its equation definition is as follows:

$$L = S * NTM \quad (5)$$

where S is the standard deviation of the CIR noise level; NTM is the noise threshold multiplier to reduce FP misjudgment caused by noise perturbation [47]. We defined the CIR stage at the receiver when the UWB signal from the transmitter has not reached the receiver as the environment noise (ENS CIR) as shown in Fig 2. This CIR waveform is relatively stable and fluctuates naturally. When the UWB signal arrives at the receiver, the CIR waveform will have abrupt jump. The system records the HTS of the first CIR that exceeds threshold L as the RFP (FP CIR) as shown in Fig. 2. Theoretically, since there is no obstacle in the LOS environment to jam the UWB signal, the RFP is the TFP. On the contrary, since the weakened TFP

XXXX-XXXX © XXXX IEEE. Personal use is permitted, but republication/redistribution requires IEEE permission.
See http://www.ieee.org/publications_standards/publications/rights/index.html for more information.

energy in the NLOS environment cannot meet threshold L, RFP arrival is later than TFP and produces a positive deviation ranging error as shown in Fig. 3. The CIR waveform after RFP is the multipath signal formed by inevitable reflection and scattering (MP CIR). In this work, the two new CCPs from the time-domain are defined as follows:

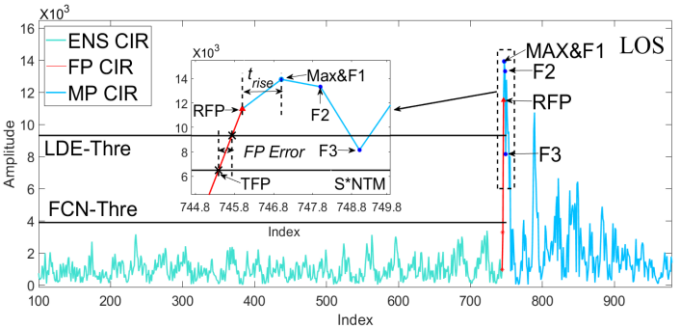

Fig. 2. Typical LOS communication process and CIR feature points.

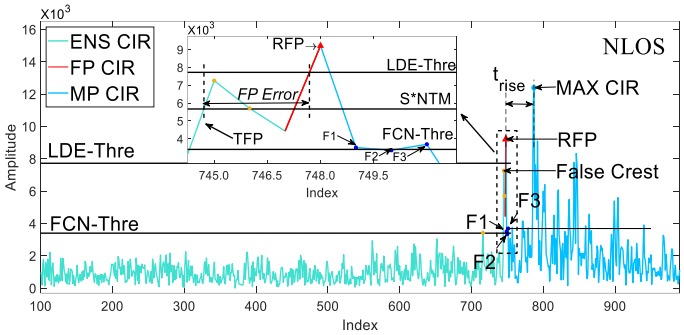

Fig. 3. Typical NLOS communication process and CIR feature points.

1) FP Error (FPE)

The difference between the weakened TFP and ambient noise in the NLOS environment is small, but the fixed and larger NTM and larger standard deviation, S, of the CIR in the NLOS environment will increase L. This will aggravate the misjudgment of FP as shown in Fig. 3. This paper provides a re-judgment of the FP by selecting a small NTM that is more suitable for the NLOS environment based on our measurement campaign. The re-judged FP is recorded as TFP, and the interpolation between it and the RFP is used as the judgment basis as follows:

$$FPE = RFP_t - \underset{t}{\operatorname{argmin}}(r(t) \geq S * NTM) \quad (6)$$

where RFP_t is the RFP arrival time. In LOS, too small NTM will result in fluctuating or abrupt environmental noise as the true mistaken UWB FP signal, while too large a value will ignore the true UWB FP signal and mistake subsequent MP signal as FP in NLOS environment. In a mixed LOS/NLOS environment, it is even more crucial to provide a reasonable performance level between false identification of noise peaks and NLOS multipath as FP during LOS and NLOS environment respectively. In this paper, NTM is optimized to 11.56 based on the 5 experimental campaign scenarios that will be conducted repeatedly 20 times each to give rise to the highest LOS/NLOS differentiation with a FPE accuracy of at least around 60 % to 73 %. The FPE in NLOS is much higher than it in LOS. In the NLOS environment, FPE is around 2.57 in Fig.3. For clear LOS, the gap between RFP_t and true FP is small with FPE around 0.38, due to the steep rise of CIR as shown in Fig. 2.

2) False Crests Number(FCN)

Both LOS and NLOS ENS contains many false crests. In addition to the false crests of natural fluctuations as shown in Fig. 2 in the LOS environment, there are many high-energy false crests in the NLOS environment as shown in Fig. 3. It is because the weakened TFP is less than threshold L and will be classified as ENS. We define the following threshold F to maximumly distinguish weakened TFP in NLOS [48]:

$$F = L * 0.6 \quad (7)$$

Under LOS, the arrival of the UWB signal will cause the CIR energy to rise sharply and be much higher than the ambient noise. As there are CIR component or points in front of the FP unless weak propagation path, the standard threshold L is suffice to distinguish ambient noise and FP. However, under NLOS, the difference between the weakened UWB FP signal and the environmental noise is subtle and the slope increase in CIR is slow. Futhermore, multipath signal may have strong energy than the true FP and be mistaken as the FP. Such misjudgement can be avoided by multiplying L by a parameter less than 1, but the size should also be controlled to avoid the misjudgements of conventional and abrupt ambient noise. In this paper, a multiplier of 0.6 is chosen based on the 5 experimental campaign scenarios that will be conducted repeatedly 20 times each to give rise to the highest LOS/NLOS differentiation with a FCN accuracy of at least around 60 % to 73 %. The number of false crests exceeding the threshold F (FCN-thre) in ENS is called False Crests Number (FCN).FCN-Thre, F is established to maximize the discovery of UWB signals before FP in NLOS, and distinguish low-energy environmental noise from high-energy UWB signals in LOS, which comes from the potential information of LDE algorithm threshold. The TFP in the NLOS environment is hidden in ENS which will increases S and more MPs are identified as FCN (=8 based on measurement campaign) in Fig. 3. In LOS, there is only fluctuating low-energy environmental noise in ENS, most FCN is equal to 0.

The traditional energy CCPs: ε_r and σ_r are calculated by the vast majority of the complete CIR dataset (1015 CIR) [47], which will increase the positioning delay. Under the same principle as FCN, the above parameters calculated by CIR in ENS have stronger performance and environmental robustness. Therefore, we use 200 CIRs before RFP to improve their performance. The new energy CCP is defined as follows:

3) FP Distance Error

According to reference[47], the first path power level (FPPL) consists of the last three CIRs of FP determined by the system. In the LOS environment, it represents the energy change caused by the real first-path UWB signal. In NLOS environment, due to the misjudgement of the system, it represents the energy of a relatively high part of the multipath signal. The sum of the squares of CIR of three-unit times {F1, F2, F3} after reported FP as shown in Fig. 2 and Fig. 3, can be used to evaluate the FPPL of the UWB signal as follows [47]:

$$FPPL = 10\log_{10}((F1^2 + F2^2 + F3^2)/PAC^2) - A \quad (8)$$

where PAC is the preamble time accumulation count in UWB measuring unit; A is the correction constant for different frequencies, which is 113.77(121.74) for 16(64) MHz [42]. Since there is no obstacle in the LOS environment, FPPL is only related to ranging distance. Based on the traditional signal attenuation model, we introduce antenna attenuation to

XXXX-XXXX © XXXX IEEE. Personal use is permitted, but republication/redistribution requires IEEE permission.
See http://www.ieee.org/publications_standards/publications/rights/index.html for more information.

establish the FPPL and distance model under LOS as follows:

$$FD = 10^{\frac{P_T+G_R+20\,log_{10}(c)-FPPL-20log10(4\pi f_R)}{20}} \quad (9)$$

where FD is fitting distance; P_T is the transmitted power; G_R=+2 dB is the total antenna gains of the transmitting and receiving antennas in the adopted UWB system [42]; f_R is the center frequency. We defined the difference between FD and the measured distance (MD) as FDE:

$$FDE = |MD - FD| \quad (10)$$

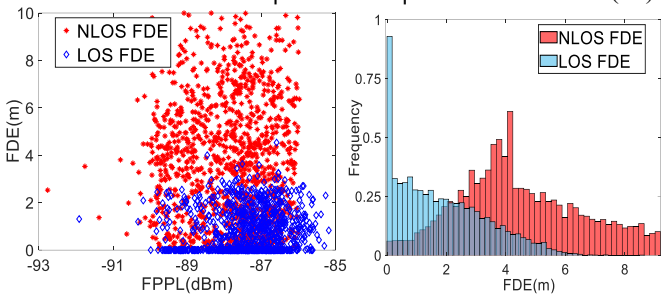

Fig. 4. FPE's different in equal FPPL and statistical distribution.

To offset the additional attenuation of the signal by obstacles under the same FPPL, the actual distance of NLOS is longer than that of LOS, so the FDE of NLOS in Fig. 4(a) is larger than LOS due to the NLOS positive ranging error. The LOS FDE in the statistical histogram Fig. 4(b) is concentrated at 1 m and below, and the mode is 0-0.3 m, which is different from NLOS.

IV. Proposed Method

A. Architecture

Fig. 5 shows the overall framework of the proposed system and data flow direction, including the membership function constructed from offline data, DTC-FCSVM identification algorithm, ranging mitigation and location of online data. Firstly, we pre-classify the data according to the correlation between multiple CCPs including our proposed CCPs with its threshold in DTC-T. Due to the classification result of some CCPs may be different from the real channel environment and shortcomings in existing LDE and the CIR waveform, we propose two typical misjudgment environments and optimize the corresponding SVM vector. Secondly, we add fuzzy credibility evaluation to the traditional SVM to form FC-SVM with better identification performance. We associate pre-classification results with the typical misjudgment environment and use different FC-SVM to finally determine whether the channel is LOS or NLOS. To improve the environmental universality of the algorithm, we use the membership function (MSF) to obtain the fuzzy credibility of parameters and optimize the classification vector. The algorithm dynamically updates DTC-T according to the final result to ensure the coarse-grained accuracy and improve the overall accuracy. During the ranging error correction stage, we classify and correct the ranging errors based on waveform characteristics and the attenuation degree of TFP energy. It can additionally modify some of the I-LOS and hence improve the identification algorithm performance. Finally, we used the corrected distance to solve the localization coordinates.

B. Fuzzy Credibility Evaluation

During the offline fuzzy mapping, we establish the MSF required by FC-SVM, which is used to determine the fuzziness of CCP. It is the probability that the parameter is judged as LOS. Fig.6 adds a description of Fuzzy Mapping in the blue frame of Fig.5, where MSF is built from a large amount of offline data via data normalization, fuzzy statistics, and membership function simulation. In red frame, the online data only use the data normalization and membership function of the Fuzzy mapping to get the fuzziness of the single CCP. Next, Main Factor method $M(\cdot,\vee)$ and Centroid method $M(\wedge,+)$ are introduced to provide the fuzziness of the CCP set, watch is used to FC-SVM.

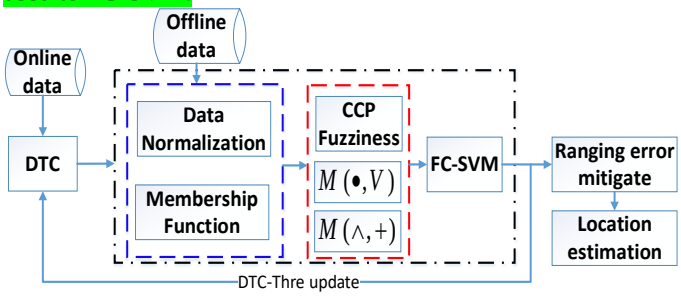

Fig. 5. The flowchart of the DTC-FCSVM algorithm.

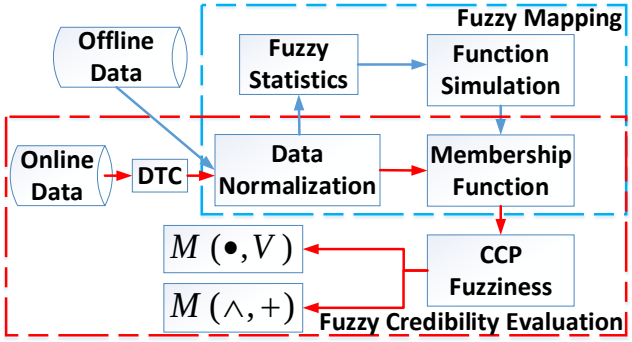

Fig. 6. Fuzzy mapping constructs membership function using offline data and the fuzzy credibility evaluation process using online data

1) Fuzzy Mapping

The basic idea of fuzzy sets [49] is to add binary decisions for absolute LOS and absolute NLOS which are represented by 1 and 0 respectively. It is expressed by the following order pair:

$$A(U) = \left\{\left(u_i, \widetilde{Los}(u_i)\right) \middle| u_i \in U\right\} i = 1,2,\cdots,I \quad (11)$$

where $U = \{u_1, u_2, \cdots, u_I\}$ is the finite set of parameters; u_i is the i^{th} CCP and I is the total number of CCPs used in the fuzzy set; $A(U)$ is the whole fuzzy set; $\widetilde{Los}(u_i)$ is the degree that u_i is judged as LOS which is obtained by the MSF in (13). The determination of MSF requires the following three steps:

(a) Data Normalization

To reduce the influence of parameters' dimensions on the final defuzzification, this paper uses the following min-max transformation to compress the original u_i within the interval [0,1]:

$$u_i' = \frac{u_{i,m} - min\{u_{i,m}\}}{max\{u_{i,m}\} - min\{u_{i.m}\}} \; m = 1,2,\cdots,M \quad (12)$$

where u_i' is the normalized value of u_i and M is the total number of data points for u_i collected in the entire offline experiment campaign.

(b) Fuzzy Statistics

XXXX-XXXX © XXXX IEEE. Personal use is permitted, but republication/redistribution requires IEEE permission.
See http://www.ieee.org/publications_standards/publications/rights/index.html for more information.

The membership degree of the fuzzy set is determined by the following statistical probability method of random events. The probability of u_i' CCP belongs to LOS (ambiguity) is determined as:

$$l_j(Los)(u_i') = \frac{\mu_{los}^j(u_i')}{\mu_{los}^j(u_i') + \mu_{Nlos}^j(u_i')} \quad (13a)$$

where $\mu_{los}^j(u_i')$ and $\mu_{Nlos}^j(u_i')$ are u_i' value being LOS and NLOS respectively in j^{th} experimental campaign trial. For example, as shown in Fig. 7(a), under LOS and NLOS environments in j^{th} trial, the normalization FDE of 0.05 has occurred approximately 80 % and 20 % of the time respectively. This translates to $\mu_{los}^j(u_i')$ and $\mu_{Nlos}^j(u_i')$ are approximately 80 % and 20 % respectively. This gives rise to $l_j(Los)(u_i')\sim 0.8$. To ensure the stability of the LOS probability prediction of each CCP, the experimental trial is repeated numerous times in which

$$l(Los)(u_i') \triangleq \frac{1}{J}\sum_{j=1}^{J} l_j(Los)(u_i') \quad (13b)$$

where $l(Los)(u_i')$ will be defined as $\widetilde{Los}(u_i)$ when J, being the number of the experimental trial is large.

(c) Function Simulation

As shown in Fig. 7, the x-axis is the u_i' of the CCP and the y-axis is the ambiguity $l(Los)(u_i')$, with the red curve being the new MSF constructed by Gaussian fitting for the three proposed CCPs. Other CCPs' MSF and more information are in [49].

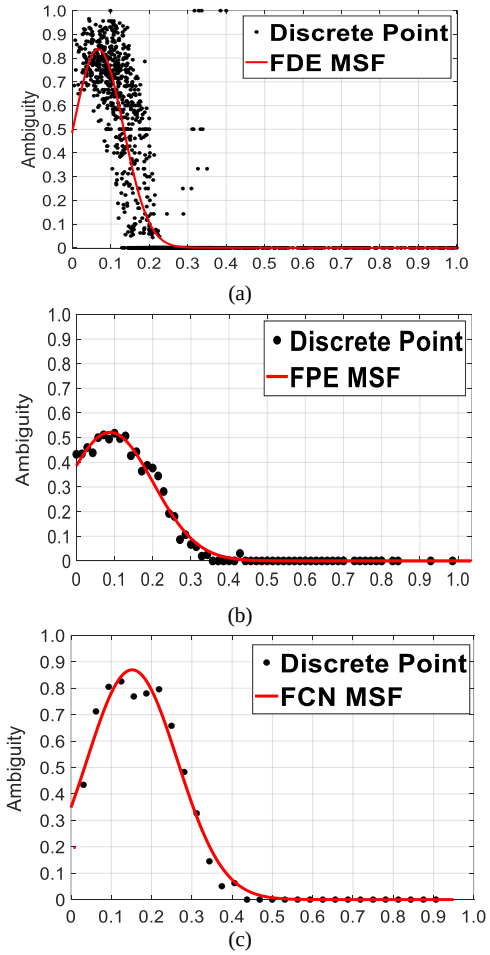

Fig. 7. The Gaussian function fits the membership functions of new CCPs. (a) FDE; (b) FPE; (c) FCN

2) Fuzzy credibility evaluation

During the online fuzzy credibility evaluation in Fig. 6, each CCP needs to be normalized similarly in the fuzzy mapping stage and fused into the corresponding MSF to obtain its fuzziness. We obtain the overall fuzzy credibility evaluation of the set through different defuzzification operations with the following model:

$$B = A' \circ R \quad (14)$$

where A' and B are two fuzzy sets of parameter domain and credibility evaluation domain, respectively; R represents the above fuzzy sets' relationship; '$\circ$' is the fuzzy operator used to obtain the evaluation results according to the information of A' and R. Suppose there are K sampling measurement set $\{g_k\}_{k=1}^K$, where each g_k has online data consisting of P dataset; g_k is further defined as part of the fuzzy set A(U):

$$g_k = U^k = \{u_i^k\}_{i=1}^I \quad (15)$$

where I is the number of CPPs as defined in (11). As such, the normalization A' of CCP from (15) is obtained as:

$$A'^k = \{u_i'^k\}_{i=1}^I = \{a_i^k\}_{i=1}^I \; 0 \le a_i \le 1 \quad (16)$$

where a_i is the normalization of u_i using (12). The credibility result B is defined as $\{b_k\}_{k=1}^K$, and the correlation matrix R is defined as $R^k = \{r_i^k\}_{i=1}^I$.

$$b_k = A'^k \circ R^k = [a_1^k, a_2^k, \cdots, a_I^k] \circ [r_1^k, r_2^k, \cdots, r_I^k] \quad (17)$$

where r_i^k is calculated differently according to different fuzzy operators. We adopt the Main Factor method $M(\cdot,\vee)$ and the Centroid method $M(\wedge,+)$ to turn fuzzy quantity into clear quantity, which is the defuzzification process [50].

(a) Main Factor method $M(\cdot,\vee)$

$$r_i^k = \widetilde{Los}(a_i^k) \quad (18)$$

$$b_k = A'^k \circ R^k = max\left\{\left(a_i^k \cdot \widetilde{Los}(a_i^k)\right)_{i=1\cdots I}\right\} \quad (19)$$

(b) Centroid method $M(\wedge,+)$

$$r_i^k = \frac{\widetilde{Los}(a_i^k)}{\sum_{i=1}^I \widetilde{Los}(a_i^k)} \quad (20)$$

$$b_k = A'^k \circ R^k = [a_1^k, a_2^k, \cdots, a_I^k] \cdot [r_1^k, r_2^k, \cdots, r_I^k] = \sum_{i=1}^I a_i^k \widetilde{Los}(a_i^k) \Big/ \sum_{i=1}^I \widetilde{Los}(a_i^k) \quad (21)$$

C. DTC-FCSVM identification

Phase 1: Dynamic Threshold Comparison

The DTC algorithm is to pre-classify the data to improve the accuracy of the final identification results. The DTC Threshold ($\{\text{dtc-}t_i\}_{i=1}^6$) is obtained offline from three empirical CCPs (PNLOS; ES; DFR) and three new proposed CCPs (FCN; FPE; FDE). This paper summarizes the obvious inconsistency between the numerical representation of some CCPs' characteristics in DTC-T and the actual channel. This consistency is named the misjudgment environment.

Since empirical CCPs focus on the multipath (MP) differences between LOS and NLOS, we proposed the introduction of a scenario where the empirical CCPs' DTC results and the actual channel are different as the misjudgment MP environment (M-MP). As shown in Table 1, there are 6 CCPs used in the proposed CCP set. For M-MP classification, PNLOS, ES, and DFR are used. Traditional LOS is defined as the intervisibility between transmitter and receiver, and it is independent of surrounding clutters and the trailing MPs. However, once the clutters around the transmitter and the

XXXX-XXXX © XXXX IEEE. Personal use is permitted, but republication/redistribution requires IEEE permission.
See http://www.ieee.org/publications_standards/publications/rights/index.html for more information.

receiver who are in LOS are heavy, the MP waveform at the receiver may be similar to NLOS. In addition, the TFP of NLOS is fully undetected in the ENS, and as such the receiver can only accept the multipath reflection signals. As such, the interval between the strongest multipath and RFP will be as small and hence PNLOS will be small. The RFP will be mistakenly treated as LOS.

The new proposed CCPs are mainly related to TFP's attenuation degree and the relationship between weakened TFP and the L. Similarly, we proposed the introduction of the misjudgment of FP as the misjudgment FP environment (M-FP) where FCN, FPE, and FDE are used. In the NLOS environment, the TFP is lower than F after path attenuation, the multipath will be misjudged as LOS due to the ENS waveform, and this phenomenon will also occur when the multipath level is higher than L. Similarly in the LOS environment, if the LOS TFP is lower than L after adding NTM, its ENS will appear the false crests like NLOS.

TABLE I
PSEUDO CODE OF THE LOS/NLOS IDENTIFICATION ALGORITHM

Algorithm: Dynamic threshold comparison LOS/NLOS identification algorithm based on UWB technology.

Input: UWB offline dataset$\{CCP_i, LOS\ or\ NLOS\}_{i=1}^{6}$, $\{CCP_i\}_{i=1}^{6}$=[FCN FPE FDE PNLOS ES DFR]^T; DTC-T {dtc-t_i}$_{i=1}^{6}$

Output: single CCP result of DTC {dtc-r_i}$_{i=1}^{6}$
DTC result {DTC-R^K }; Final result{$Result^K$}

For k=1 to K
Compare $\{CCP_i\}_{i=1}^{6}$ with the corresponding {dtc-t_i}$_{i=1}^{6}$ to get{dtc-r_i}$_{i=1}^{6}$. LOS: dtc-r_i^k=1; NLOS: dtc-r_i^k=0;
Due to the correlation between CCPs, $dtc - r_{4:5}^k$ needs to be corrected
  if CCP_5^k < 0.1 & dtc-r_4^k==1;
    dtc-$r_{4:5}^k = 0$
  end
  Calculate the sum of {dtc-r_i^k}$_{i=1}^{6}$ to get DTC-R^K.
  The $Result^k$ = 1/0 when DTC-R^k=6/0.
  if sum (dtc-$r_{i=1:3}^k$)<3
    $Result^k$ = M-MP label class
  else if sum(dtc-$r_{i=1:3}^k$)>3& DTC-R^k = 4 or 3 or 2
    $Result^k$ = Mixture of M-MP & M-FP label class
  else
    $Result^k$ = M-FP label class
  end
The data $Result^k \neq$ 1/0 needs to be fine-grained identified with FC-SVM to get the final $Result^k$.
The data with $Result^k$=1 will be added in DTC-D, and the DTC-T will be updated every 30 time-series data
end

The formulation of the DTC-threshold (DTC-T) initialization and update rules are as follows:

a) Threshold Initialization (Offline)

Firstly, the first and last 3 % of the sorted offline dataset of each CCP value are removed and the remaining dataset is termed as DTC-Decision (DTC-D) dataset. The value at the 90 % percentile of the DTC-D dataset is used as the initialization dtc-t_i, and restored in DTC-T. However, we need to repeat the above initialization operation if ES<0.9 or PNLOS<0.5 or DFR≥6 dB [48].

b) Threshold Update (Online)

During online update process, as shown in Fig. 5, if every 30 time-series online datasets have been identified by FC-SVM as the LOS class, they will be added into the DTC-D dataset to repeat the initialization operation to update the dtc-t_i in DTC-T. However, if these LOS datasets did not meet the ES, PNLOS, and DFR criteria as mentioned in step a), these LOS data will not be added to the DTC-D dataset to update the DTC-T.

The CCP_i^k represents the k^{th} data of dataset and the i^{th} CCP of [FCN, FPE, FDE, PNLOS, ES, DFR]". The first three CCPs correspond to the proposed CCP that are deived from the proposed three stages of UWB signal acquisition. During DTC process, we compare CCP_i with the dtc-t_i in DTC-T, and if CCPs (except ES and PNLOS) are less than the threshold, we will indicate this result as dtc-r_i = 1, else as 0. The operation of CCPs ES and PNLOS is the opposite. According to this threshold judgment process of a single CCP and hence for all CCPs, the pseudo-codes in Table 1 are used in data threshold pre-classification.

Phase 2: Fuzzy credibility-based SVM

The coarse-grained classification performance in Phase 1 has poor robustness to environments and will be affected by human movement. In this paper, we extend the FSVM [51, 52] classifier to fine-tune the classification of the DTC results with our proposed fuzzy credibility into FC-SVM.

To get better classification results, FC-SVM first maps the input points $(x_1, y_1), (x_2, y_2), \cdots, (x_K, y_K)$ to high-dimensional feature space where $\boldsymbol{x}$ is the feature vector and $y = \{-1, +1\}$ is the channel environment as NLOS or LOS respectively. The classifier divided data into two types according to the hyperplane of this space, which can be expressed as:

$$\boldsymbol{w}^T \Phi(\boldsymbol{x}) + w_o = 0 \tag{22}$$

where Φ is the mapping function; w_0 is the bias. The system finds the above separation hyperplane by solving the following maximum margin optimization problem:

$$argmin\ \frac{1}{2}||\boldsymbol{w}||^2 + \gamma \sum_{k=1}^{K} \xi_k \tag{23}$$

where γ controls the trade-off between minimizing training errors and model complexity; $\xi_k > 0$ are slack variables that allow the SVM to tolerate misclassifications. The solution is the quadratic optimization using Lagrange duality

$$MaxW(\lambda) = \sum_{k=1}^{K} \lambda_k - \frac{1}{2} \sum_{k=1}^{K} \sum_{j=1}^{K} \lambda_j \lambda_k y_j y_k \Phi(\boldsymbol{x_j}) \Phi(\boldsymbol{x_k}) \tag{24}$$

where λ_k is the Lagrange multiplier satisfying Karush-Kuhn-Tunker (KKT) and $0 \leq \lambda_k \leq \gamma$; γ can be considered as the misclassification cost value, the more important ξ_k are assigned higher costs:

$$\lambda_k(y_k(\boldsymbol{w}^T \Phi(\boldsymbol{x}) + w_o) - 1) + \eta_k \xi_k) = 0 \tag{25}$$

Another advantage of SVM is to use kernel function K(x,y)=$\Phi(x)\Phi(y)$ or other point functions instead of mapping equation $\Phi(x)$, and the dual-optimization problem in (24) can be transformed into:

$$MaxW(\lambda) = \sum_{k=1}^{K} \lambda_k - \frac{1}{2} \sum_{k=1}^{K} \sum_{j=1}^{K} \lambda_k \lambda_j y_k y_j K(\boldsymbol{x_k}, \boldsymbol{x_j}) \tag{26}$$

The optimal value of λ_k can be obtained by solving (26), and w can be expressed as:

$$w = \sum_{k=1}^{K} \lambda_k y_k \Phi(\boldsymbol{x_k}) \tag{27}$$

The support vectors are the data points with nonzero λ_k value and the result can be written as:

$$l(x) = sign(\boldsymbol{w}^T \Phi(\boldsymbol{x}) + w_0)$$

XXXX-XXXX © XXXX IEEE. Personal use is permitted, but republication/redistribution requires IEEE permission.
See http://www.ieee.org/publications_standards/publications/rights/index.html for more information.

$$= sign\left[\sum_{k=1}^{K} \lambda_k y_k K(\boldsymbol{x_k}, \boldsymbol{x}) + w_0\right] \quad (28)$$

Next, we determine the optimal feature set to be used in the proposed FC-SVM classifier in different scenarios. The classification performance of empirical model parameters is poor in CCP classification which includes various CCPs such ε_r, σ_r, τ_{MED}, κ, and t_{rise}. Aiming at the two misjudgment environments that we have proposed namely M-MP and M-FP, we further propose its corresponding classifiers FCSVM_{MP} and FCSVM_{FP} whose feature sets include the three proposed CCPs are shown in TABLE II. The proposed FC-SVM additionally introduces the fuzzy credibility M(·,∨) and M(∧,+) of the whole CCP set to optimize results further. Moreover, we propose another $\text{FCSVM}_{\text{Entire}}$ to further process the data whose pre-classification result is a mixture of M-FP & M-MP in some cases. When the pre-classification result is a mixture of M-FP & M-MP, both classifiers FCSVM_{MP} and FCSVM_{FP} will be used. If the recognition results obtained by FCSVM_{MP} and FCSVM_{FP} are consistently the same, it will be regarded as the final result. Else, the final result needs to be determined by $\text{FCSVM}_{\text{Entire}}$ with its optimal CCPs set is also in TABLE II:

TABLE II
CLASSIFIER AND CORRESPONDING PARAMETERS

	Feature vector X
FCSVM_{MP}	$X_{MP} = [FPE, FCN, FDE, \varepsilon_r, \sigma_r, M(\cdot,\vee), M(\wedge,+)]^T$
FCSVM_{FP}	$X_{FP} = [ES, DFR, \tau_{MED}, \kappa, t_{rise}, M(\cdot,\vee), M(\wedge,+)]^T$
FCSVM_{Entire}	$X_{Entire} = [FPE, FDE, DFR, \tau_{MED}, \kappa, t_{rise}, \sigma_r, M(\cdot,\vee), M(\wedge,+)]^T$

D. Ranging error compensation and position estimation

In NLOS conditions, TFP is weakened by obstacles or hidden in ENS. It is recorded in S of (5), which increases L and causes the RFP used to calculate TOF to be later than TFP, resulting in a positive offset-ranging error. Traditionally, location methods that combined corrected I-NLOS and I-LOS ranging have the following problems. Firstly, some NLOS data being included in the I-LOS due to the recall of LOS cannot reach 100 %. Secondly, the existing TFP estimation techniques are complex and time-consuming. According to the attenuation degrees of TFP in Fig. 8, we take the FCN=0 as the boundary to distinguish the difficulty of identifying TFP. As shown in Fig. 8, there are two typical scenarios. As such, TFP estimation and TFP energy back-calculation correction algorithms are used respectively.

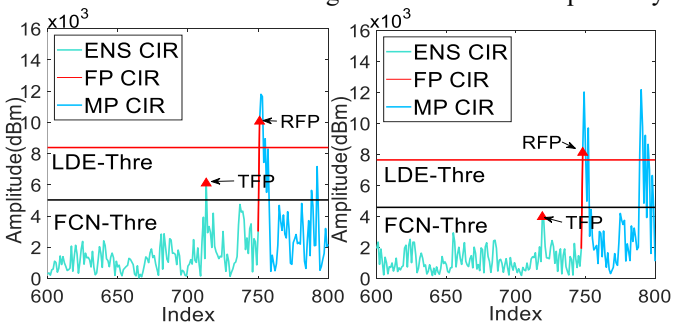

Fig. 8. NLOS waveforms with two different TFP weakening degrees.

1) TFP estimation

The CIR of the weakened TFP in Fig. 8(a) is significantly different from that of the ENS and higher than FCN-Thre, F. At this point, the ranging error with FCN>0 is due to fixed NTM in LDE, which cannot differentiate the TFP. The error model is as follows:

$$\tilde{d} = \hat{d} - \Delta d_{FCN>0} \quad (29)$$

where $\tilde{d}$ and $\hat{d}$ represent the corrected and measured distances, respectively; $\Delta d_{FCN>0}$ is the ranging correction value. The ranging correction value is based on the difference between the real FP and the measured FP of the arrival time of POLL, RESP and FINAL signals as shown in Fig.1. Eq. (6) is used to re-judge FP and use this proposed FPE to measure the above difference and bring into Eq. (1) and Eq. (2). According to [12, 53, 54], the $\Delta d_{FCN>0}$ is formed as shown in equation (30):

$$\begin{aligned}\Delta d_{FCN>0} &= f(e,\hat{d}) = c * \Delta tof = c * (\widehat{tof} - tof) \\ &= c * \frac{e(slot+e)}{2slot} + \frac{(slot-e)}{slot}\hat{d}\end{aligned} \quad (30)$$

where $e = FPE * timestamp\ resolution$[47] and slot is the 2 way round trip transmission time value as obtained in Fig. 1 ; $\widehat{tof}$, tof and Δtof represent measured time of flight, true time of flight, and the difference between $\widehat{tof}$ and tof, respectively. The proposed TFP estimation algorithm in (30) can correct both true LOS under M-FP and some NLOS misjudgment in I-LOS

2) TFP energy back-calculation

As shown in Fig. 8(b), the difference between the weakened TFP below F and ENS is small. We need to introduce additional parameters in the error correction with the following proposed model:

$$\tilde{d} = \hat{d} - \Delta d_{FCN=0} \quad (31)$$

where $\Delta d_{FCN=0}$ is the ranging correction. In this scenario, our proposed CCP, namely the FPE can find the signal arrival time closer to TFP, which is an NLOS multipath signal. In this case, we adopt the weighted least squares algorithm combined with FPE and the FP energy with the proposed model as:

$$\begin{aligned}\Delta d_{FCN=0} &= g(f(e,\hat{d}), FDE, \beta_0, \beta_1) \\ &= \beta_0 * f(e,\hat{d}) + \beta_1 * FDE + \varepsilon \\ &= \beta_0 X1 + \beta_1 X2 + \varepsilon, , \varepsilon \sim n(0,\sigma^2)\end{aligned} \quad (32)$$

where $X1$ and $X2$ are matrix representations of the FPE and FDE respectively with β_0 and β_1 as their respective coefficient. The matrix expression of (32) is:

$$\mathbf{y} = \mathbf{Xb} + \boldsymbol{z} \quad (33)$$

$$\mathbf{X} = \begin{bmatrix} X_{11} & X_{12} \\ X_{21} & X_{22} \\ \vdots & \\ X_{P1} & X_{P2} \end{bmatrix}, \mathbf{y} = \begin{bmatrix} \Delta d_{FCN=0}^{nlos_1} \\ \Delta d_{FCN=0}^{nlos_2} \\ \vdots \\ \Delta d_{FCN=0}^{nlos_P} \end{bmatrix}, \mathbf{b} = \begin{bmatrix} \beta_0 \\ \beta_1 \end{bmatrix}, \mathbf{z} = \begin{bmatrix} \varepsilon_1 \\ \varepsilon_2 \\ \vdots \\ \varepsilon_P \end{bmatrix} \quad (34)$$

where P is the number of offline measurements between anchor and tag. The pseudo-inverse least square solution of (34) is :

$$\mathbf{b} = (\mathbf{X}^T\mathbf{X})^{-1}\mathbf{X}^T\mathbf{y} \quad (35)$$

where $\mathbf{y}$ is obtained from offline measurement campaigns in various environments.

Based on waveform analysis, we use the following proposed model to re-calibrate the whole I-NLOS and part of I-LOS with FCN>0.

$$\begin{cases} LOS & \begin{cases} FCN = 0 & \tilde{d} = \hat{d} \\ FCN > 0 & \tilde{d} = \hat{d} - f(e,\hat{d}) \end{cases} \\ NLOS & \begin{cases} FCN = 0 & \tilde{d} = \hat{d} - g(f(e,\hat{d}), FDE, \beta_0, \beta_1) \\ FCN > 0 & \tilde{d} = \hat{d} - f(e,\hat{d}) \end{cases} \end{cases} \quad (36)$$

3) Position estimation

After obtaining the corrected ranging results, $\tilde{d}$, the position

XXXX-XXXX © XXXX IEEE. Personal use is permitted, but republication/redistribution requires IEEE permission.
See http://www.ieee.org/publications_standards/publications/rights/index.html for more information.

is solved by the pseudo-inverse least square solution to further suppress the influence of ranging error on positioning accuracy. The coordinates of the anchors and the tag are $(x_1, y_1); (x_2, y_2); \cdots; (x_N, y_N)\ N \geq 3$ and (x_0, y_0) respectively; The distances between the tag and different anchors are calculated by the following formula is $\{\tilde{d}_n\}, n = 1,2, \cdots, N$:

$$\tilde{d}_n = \sqrt[2]{(x_n - x_0)^2 + (y_n - y_0)^2} \tag{37}$$

Written in matrix form:

$$\mathbf{b}_{(N-1)x1} = \begin{bmatrix} \tilde{d}_1^2 - x_1^2 - y_1^2 - \tilde{d}_N^2 + x_n^2 + y_n^2 \\ \tilde{d}_2^2 - x_2^2 - y_2^2 - \tilde{d}_N^2 + x_n^2 + y_n^2 \\ \vdots \\ \tilde{d}_{N-1}^2 - x_{N-1}^2 - y_{N-1}^2 - \hat{d}_N^2 + x_N^2 + y_n^2 \end{bmatrix} = \begin{bmatrix} b_1 \\ b_2 \\ \vdots \\ b_{N-1} \end{bmatrix} \tag{38}$$

$$\mathbf{A}_{(N-1)x2} = -2 \begin{bmatrix} x_1 - x_N & y_1 - y_N \\ x_2 - x_N & y_2 - y_N \\ \vdots & \vdots \\ x_{N-1} - x_N & y_{N-1} - y_N \end{bmatrix} \tag{39}$$

$$\mathbf{p}_{2x1} = \begin{bmatrix} x_0 \\ y_0 \end{bmatrix} \tag{40}$$

To obtain $argmin||\mathbf{Ap} - \mathbf{b}||_2^2$

$$||\mathbf{Ap} - \mathbf{b}||_2^2 = \mathbf{p}^T\mathbf{A}^T\mathbf{Ap} - 2\mathbf{p}^T\mathbf{A}^T\mathbf{b} + \mathbf{b}^T\mathbf{b} \tag{41}$$

Equating to 0, the optimal global solution will be:

$$\mathbf{p} = (\mathbf{A}^T\mathbf{A})^{-1}\mathbf{A}^T\mathbf{b} \tag{42}$$

V. Experiments

A. Experimental Setup

To verify the performance of the proposed NLOS/LOS identification and ranging error correction algorithms, Decawave DW1000 UWB module system based on IEEE802.15.4-2011 has been used. The UWB system has also been configured to send the parameter data to the mobile phone acquisition software in real time. Its effective communication distance is 50 m, communication rate is 110 kb/s, transmission power is -41.3 dBm/MHz with operating center frequency as 3.5 GHz. Experimental campaigns in various test scenarios are conducted at the UWB test site of the School of Environment and Spatial Informatics, China University of Mining and Technology (CUMT), and State Key Laboratory of Satellite Navigation System and Equipment Technology, 54th Research Institute of China Electronics Technology Group Corporation (LAB) as shown in Fig. 9 (a)&(b) and Fig. 9 (c)&(d). The distances between the anchor and tag pairs are shown in TABLE III.

TABLE III
THE DISTANCE BETWEEN THE ANCHOR AND THE TAG IN FIVE SCENARIOS

	Location	Obstacle	Distance
STA-1	CUMT	Human	[1.096,3.147,5.128,6.126,7.143,8.155, 9.181,10.203]
STA-2	CUMT	Wall	[3.370,5.370,7.370,9.370,11.370, 13.370,15.370]
STA-3	CUMT	Mix	[5.525,6.521,8.126,10.054,12.151, 14.343,16.593,18.879]
STA-4	LAB	Human	[1.237,2.421,3.666,4.833,6.042,7.236, 8.426,9.603,10.868]
STA-5	LAB	Glass	[1.644,2.864,4.064,5.264,6.464,7.664]

As shown, Fig. 9 (a) and Fig. 9 (b) are office environment of 30.90 m x 36.20 m using cartesian coordinate system of relative coordinates while Fig. 9(c) and Fig. 9 (d) are a typical 3-level building of 24.00 m x 30.50 m to mimic a commercial building such as shopping mall. Fig.9 (a) and Fig.9 (c) depict LOS scenarios in the two environments while Fig 9 (b) and Fig. 9 (d) depict the NLOS scenarios in the two environments. The obstacle of STA-2 in Fig. 9 (b) is a single wall (Wall I), and the obstacle of STA-3 is a group of walls (Wall II, Wall III and Wall IV). All walls are made of reinforced concrete and their thickness is in order 0.20 m, 0.23 m, 0.20 m and 0.24 m respectively. In Fig. 9(d), the material of the obstacle in STA-5 is tempered frosted glass and its thickness is 0.13 m. The red and blue marks in Fig.9 represent the location of anchors and tags respectively. Fig. 9 (a) and Fig. 9 (b) experimental campaign are mainly groups of static experiment with the tag having incremental movement one at a time, and its distance from the fixed anchor is recorded in TABLE III. Fig. 9 (c) and Fig.9 (d) includes dynamic tag trajectory to measure the accuracy of the proposed UWB system in motion. In addition, the tag's position in STA-2 coincides with the anchor's position in STA-3 in Fig.9 (b). Under the China national standard requirement of centimetres accuracy imposed on the UWB localization system, the ground truth must be measured with millimetres resolution. However, the measuring tape can only provide centimetres measurement resolution with parallax error in human reading. Furthermore, considering ground unevenness and the distance between the UWB tag and anchor is measured in the mid-air rather than on the ground as shown in Fig.9 (d), the measuring tape will suffer bending due to gravity when the distance measurement is too long in the experimental campaign area. Therefore, the measuring tape was used on the ground to determine the approximate distance between the anchor and the tag as shown in Fig.9 (d). The laser rangefinder Leica DISTO D510 [55] which has average ranging error of ± 1.0 mm, a maximum ranging error of ± 2.0 mm and a range of 200 m is then employed to provide high accuracy ground truth. As shown in Fig.9 (d), the anchor and the tag are aligned to each other so that the laser emitted by the laser rangefinder at the anchor reaches the tag surface at the right angle so that Time of Flight is measured accurately by the laser rangefinder to provide the exact real distance between the tag and anchor. In summary, in the experimental measurement campaign, the ground truth is firstly approximated by the measuring tape to determine the approximate location of the tag and baseline distance between the tag and anchor. This is followed by precise pinpoint of the ground truth by the laser rangefinder through the measurement of the distance between the tag and anchor five times and take the averages as the real distance. This real distance will use to verify the measured distance performed by the proposed UWB system. The two environments are mainly Rician and Rayleigh channel in nature for LOS and NLOS scenarios respectively. In the data acquisition process of STA-1&4, we collect LOS data first and keep the anchor and tag position unchanged to collect NLOS human interference data. 10 minutes of CIR data collection is obtained for each pair of anchor and tag distance at a resolution of 50 LOS CIR data/minute and 50 NLOS CIR data/minute totaling 100 CIR/minute at each point. As shown in Fig.9, there are myriad obstacles between the STA-3 anchor and tags such as walls, wooden doors, and various room furniture, namely mix. In STA-2, 3 & 5 experimental campaigns, with corresponding obstacles wall, mix, and glass, as the anchor and

XXXX-XXXX © XXXX IEEE. Personal use is permitted, but republication/redistribution requires IEEE permission.
See http://www.ieee.org/publications_standards/publications/rights/index.html for more information.

all tags are in NLOS with each other, we also simultaneously position another LOS tag that is having the same distance separation to the anchor, equidistant with the NLOS tag to the same anchor. This facilitates the collection of both LOS and NLOS data. The training and testing data set was split into 70: 30 that is arisen from these acquired data to obtain the existing and proposed CCPs (FPE, FCN, FDE) using.

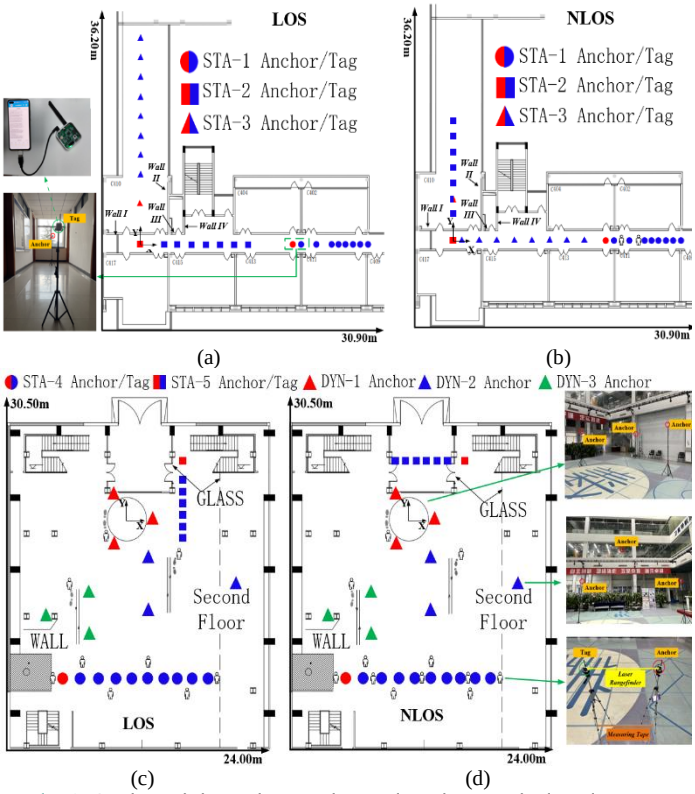

Fig. 9. Static and dynamic experimental equipment devices layout.

B. LOS/NLOS identification performance

We use the following equations to evaluate the identification accuracy:

$$Accuracy = \frac{LR + NR}{LR + NR + LW + NW} \quad (43)$$

$$Recall_{LOS} = \frac{LR}{LR + LW} \quad (44)$$

$$Recall_{NLOS} = \frac{NR}{NR + NW} \quad (45)$$

where LR/NR is the number of data correctly identified as LOS/NLOS; LW/NW is the corresponding misjudgment data for LOS/NLOS. The above parameters are overall recognition accuracy, LOS recall, and NLOS recall.

1) SVM identification accuracy with signal CCP

As shown in TABLE IV for the identification accuracy of the single CCP with a standard LS-SVM [16] in various scenarios, the proposed CCP's performances (FPE, FDE, and FCN) are generally outperformed all existing CCPs. As shown, existing CCPs suffer inconsistent performance throughout the 5 experimental campaigns while the proposed CCPs' performances are robust and consistent in all 5 experimental campaigns. One of the proposed CCPs always has the best accuracy in these 5 experimental campaigns and the remaining two CCPs are within approximately 10 % accuracy performance from the best achiever as compared to existing CCPs.

TABLE IV
THE RECOGNITION ACCURACY OF THE SINGLE PARAMETER

CCP \ Scene	STA-1 (Scene 1)	STA-2 (Scene 2)	STA-3 (Scene 3)	STA-4 (Scene 4)	STA-5 (Scene 5)
DFR	62.67 %	68.74 %	50.69 %	63.00 %	65.94 %
t_{rise}	63.02 %	60.64 %	50.69 %	66.28 %	75.50 %
ε_r	38.03 %	41.77 %	29.33 %	55.87 %	56.79 %
σ_r	61.98 %	60.30 %	50.69 %	60.72 %	57.33 %
κ	61.98 %	58.24 %	51.69 %	78.26 %	65.40 %
ES	65.61 %	61.74 %	50.69 %	70.05 %	62.75 %
τ_{MED}	61.98 %	58.24 %	51.69 %	65.66 %	64.64 %
FPE	63.65 %	64.30 %	59.69 %	73.26 %	68.89 %
FDE	67.68 %	70.82 %	59.69 %	82.58 %	77.41 %
FCN	64.99 %	65.64 %	59.69 %	72.75 %	67.04 %

2)DTC-FCSVM identification accuracy

Next, we investigate the performance of the proposed DTC-FCSVM algorithm in LOS/NLOS identification in these 5 different scenarios. The result is illustrated in Fig. 10. Our proposed DTC-FCSVM has the highest mean accuracy of about 93.27 % in all scenarios as compared to LS-SVM and KNN. The mean Recall LOS is about 94.27 % as compared to LS-SVM of 80.33 % in LOS identification. As shown, the Recall NLOS for DTC-FCSVM is guaranteed to be above 90 % with a mean of 92.57 % as compared to LS-SVM and KNN of 89 % and 76 % respectively.

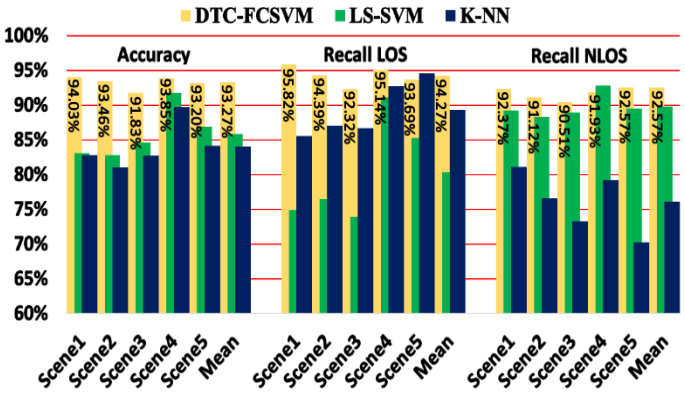

Fig. 10. Three algorithms' classification performance in five scenarios. The percent numbers are the accuracy of DTC-FCSVM. We use the same identification vector $\{\varepsilon_r, \kappa, t_{rise}\}$ as that used in [25]. The feature vector of K-NN is the same as [30].

C. Ranging mitigation evaluation

Contrary to traditional algorithms that focus on the correction of I-NLOS data, our algorithm is capable in the correction of both I-NLOS and partial I-LOS data. We evaluate the measured correction performance using mean, standard deviation (STD), and root means square error (RMSE). These two types of data correction effects are illustrated in TABLE V and TABLE VI, respectively.

Existing algorithms do not correct I-LOS data, but from TABLE V, it is noteworthy to observe the importance to correct I-LOS errors as the error correction improvement is more than 40 %. Fig. 11 illustrates the LOS CDF of original LOS ranging error (OE-LOS), DTC-FCSVM predicted LOS classification error (PE-LOS), and mitigated LOS error (ME-LOS) using ranging error compensation in section D. As shown, the CDF

XXXX-XXXX © XXXX IEEE. Personal use is permitted, but republication/redistribution requires IEEE permission.
See http://www.ieee.org/publications_standards/publications/rights/index.html for more information.

performance of the ME-LOS is more than 90 % at ranging error less than 0.5 m in all scenarios and outperforms the raw OE-LOS without correction and PE-LOS after DTC-FCSVM LOS classification.

TABLE V
ERROR CORRECTION EFFECT IN DIFFERENT SCENARIOS OF I-LOS

	Mean(m)		STD(m)		RMS(m)	
	Original	Mitigate	Original	Mitigate	Mitigate	Mitigate
Scene1	0.0407	0.0288	0.1115	0.0628	0.1187	0.0691
Scene2	0.0422	0.0282	0.1299	0.0617	0.1366	0.0678
Scene3	0.0542	0.0317	0.1437	0.0653	0.1536	0.0726
Scene4	0.1409	0.0714	0.4145	0.2358	0.4377	0.2464
Scene5	0.1068	0.0630	0.3603	0.2043	0.3760	0.2138

TABLE VI
ERROR CORRECTION EFFECT IN DIFFERENT SCENARIOS OF I-NLOS

	Mean(m)		STD(m)		RMS(m)	
	Original	Mitigate	Original	Original	Mitigate	Original
Scene1	1.1262	0.6305	1.6898	0.9652	2.0306	1.1528
Scene2	1.2468	0.5762	1.6519	0.7532	2.0695	0.9482
Scene3	1.1194	0.6505	1.1738	0.8848	1.6219	1.0981
Scene4	2.7985	1.1895	4.4284	1.8082	5.2380	2.1642
Scene5	0.8421	0.4498	1.4278	0.8341	1.6575	0.9476

Similarly, as shown in TABLE VI, our proposed ranging error compensation algorithm outperforms OE-NLOS and PE-NLOS with a reduction of the STD and RMSE by an average of 44.53 % and 46.24 % respectively. It is noteworthy to observe more than 53 % improvement when the NLOS environment is severe, demonstrating the excellent performance and robustness of the proposed ranging error compensation algorithm. Fig. 12, also demonstrates the CDF out performance and robustness of the proposed ME-NLOS ranging error compensation algorithm, achieving 90 % CDF in all scenarios except scenarios 4 and 5. Scenario 4 has the most severe NLOS environment with various obstacles and human interaction. It has at most 80 % CDF at the ranging error of fewer than 2.5 m but nevertheless the mean, STD, and RMSE are improved by 57.50 %, 59.17 %, and 58.68 %, respectively using ME-NLOS as compared to PE-NLOS. In scenario 5, the UWB signal is refracted through the glass as a blocked LOS path (NLOS) with refraction loss and minimum ranging error.

It is interesting to note the impact of human presence and obstacle in STA-4 error in Table V and VI. In LOS scenarios in Table V, the human group in the proximity of the STA-4 anchor and tag, causing some Fresnel zone phenomenon and constituting in comparable multipath caused by human reflection/diffraction to the receivable LOS component. This resulted its LOS error correction performance is slightly inferior as compared to the scenarios STA-5 where there is no human movement except glass and wall obstacles. The operating UWB center frequency is 3.5 GHz, and both anchor and tag are positioned at a height of 1.5 m causing some Fresnel radius of between 15.32 cm and 63.6 cm. In NLOS scenarios of STA-4, the human obstacle effect is exacerbated since there is a human obstacle in between the anchor and tag in addition of surrounding human. Human has a higher dielectric constant that causes high signal attenuation as compared to the glass obstacles in the STA-5 NLOS scenarios. However, our proposed mitigation scheme has helped to reduce such human effect error tremendously as shown in Table V and VI.

As shown in Fig. 13, the average LOS and NLOS max errors are reduced by 0.229 m (9.53 %) and 1.880 m (44.71 %) respectively as compared to the original dataset. Fig. 14 shows the different algorithms' ranging error optimization in multiple scenarios. The corrected mean error of the proposed ranging mitigation algorithm is better than traditional LS-SVM[25] and K-NN[30] in all scenarios. On STD and RMSE performance indicators, only LS-SVM in Scene 4 is slightly better than the proposed ranging mitigation, while K-NN perform unsatisfactory in all scenarios. In summary, the proposed ranging mitigation algorithm has demonstrated better robustness and correction effect as compared to traditional LS-SVM and K-NN. Fig. 15 depicts the Cumulative Distribution Function (CDF) of the ranging errors between Ranging Mitigation in this paper and those in KNN and LS-SVM. As shown, LS-SVM algorithm outperforms both KNN and LS-SVM in all scenarios, achieving around or less than 1m for 90 % of the times.

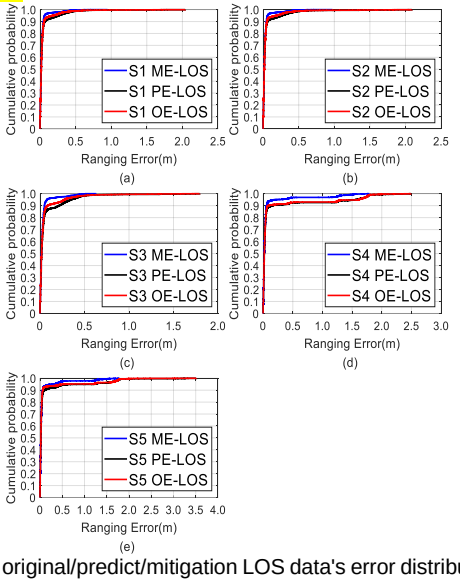

Fig.11. The original/predict/mitigation LOS data's error distribution under five scenarios and obstacles. In CUMT, the obstacles of three experiments are (a) Human; (b) Mix; (c)Wall (d) Human/Mix; (e) Glass.

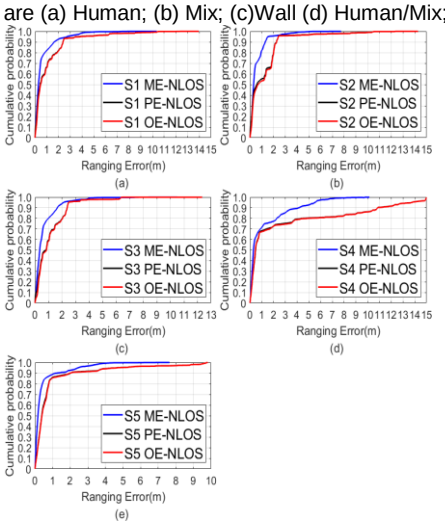

Fig.12. Under different scenarios and obstacles, the original/recognized/mitigation NLOS data's error distribution. a) Human; (b) Mix; (c)Wall (d) Human/Mix; (e) Glass are in LAB.

XXXX-XXXX © XXXX IEEE. Personal use is permitted, but republication/redistribution requires IEEE permission.
See http://www.ieee.org/publications_standards/publications/rights/index.html for more information.

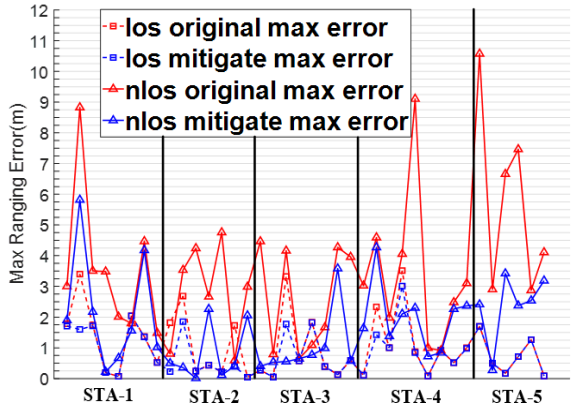

Fig. 13. Maximum error correction effect of all distances in five scenes.

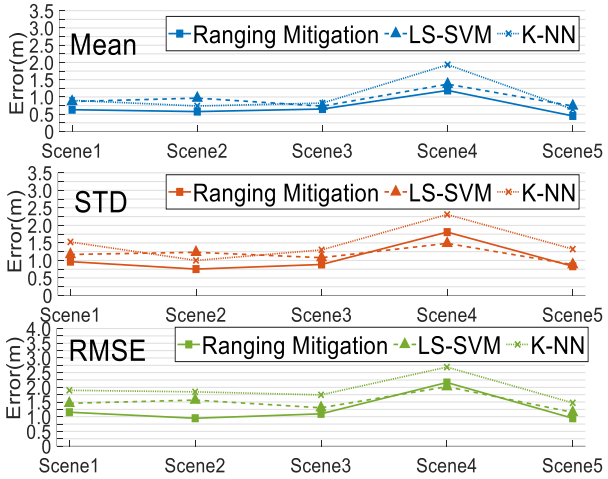

Fig. 14. Three algorithms' error correction performance in five scenes. The ranging mitigation vector of LS-SVM is $\{\varepsilon_r, \kappa, t_{rise}, \tau_{MED}, \tau_{rms}, \tilde{d}\}$ [25]. The feature vector of K-NN is the same as [30].

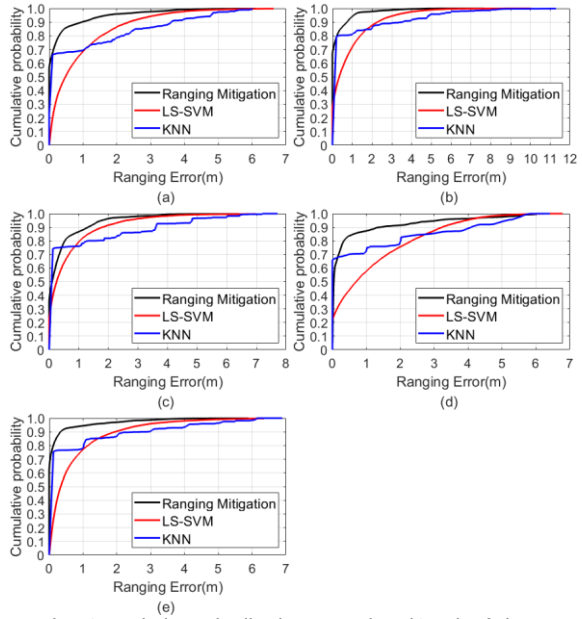

Fig. 15. The Cumulative Distribution Function (CDF) of three ranging mitigation algorithms in five scenes.

D. Positioning experiment

To verify the improvement of positioning accuracy by the DTC-FCSVM identification algorithm and ranging error correction with position estimation, we set up three groups of obstacle experiments (Human, Glass, and Wall) on the LAB in Fig. 16, namely DYN-1-DYN-3 in Fig 9(b). In DYN-1 (S1), the anchors are fixed on the LAB's first floor along the reference trajectory (RT) as shown in Fig. 16(a). Due to human blockage, the deviation between the original trajectory (OT) and the RT is much higher than the mitigated trajectory (MT) using the proposed algorithm (DTC-FCSVM + Ranging Mitigation + Positioning). It is worth noting that although the LOS OT in the lower right corner of Fig. 16(a) highly coincides with RT, our proposed algorithm can provide better and further correction and improvement effect. In Scene 2, the tester raised the tag to ensure that there is always a Glass obstacle between the tag and the second-floor anchor during the formation of Fig. 16(b)'s RT without much human interference. As the UWB signal communication between the tag and anchor is only mainly obstructed by glass penetration, the OT's deviation is very small due to strong LOS signal penetration through glass and the MT is basically consistent with the RT. The proposed algorithm reduces the positioning error from 0.576 m to 0.148 m achieving 74.3 % improvement. In Fig. 16(c), there is a wall obstacle at one of the anchors. This results in positive deviation ranging error due to strong NLOS. Most of the OT points are located on the right side of the RT. After correction with the proposed algorithm, all positioning errors are less than 1 m. As shown in Fig. 16(d), the average CDF error performance using proposed algorithm for the three scenarios outperforms the original trajectory positioning by more than 40 % at error less than 0.4 m. The Mean and Max errors are reduced by more than 60 %, while the STD is reduced by 55 %. Compared with the KNN, the proposed DTC-FCSVM reduces the positioning error of Mean, STD and RMSE by 42.79 %, 28.34 % and 13.19 %, respectively. Compared with LS-SVM, the proposed algorithm outperformed by 50.45 %, 28.40 % and 35.79 % in mean, standard deviation and RMSE. The detailed performance of the proposed algorithm for the 3 sets of experimental setup is shown in TABLE VII.

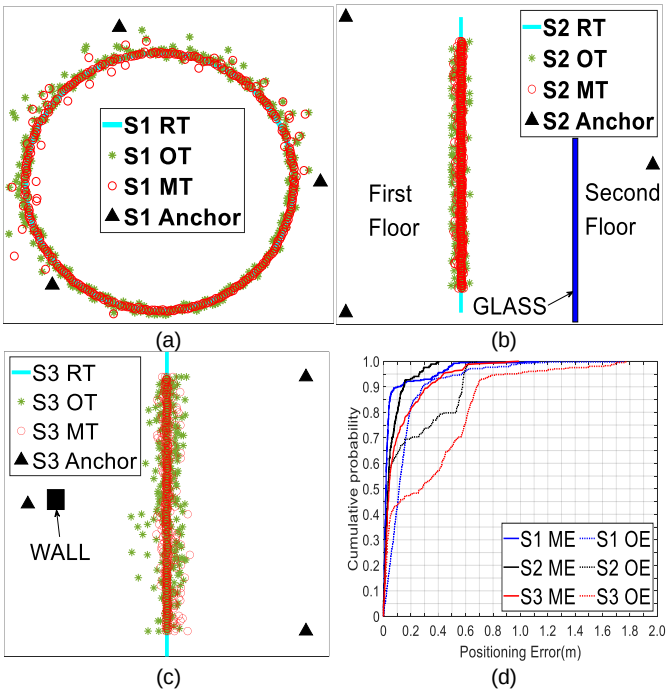

Fig. 16. Dynamic positioning experiment and error distribution in three obstacle scenes. a) Human; b) Glass; c) Wall; d) CDF.

XXXX-XXXX © XXXX IEEE. Personal use is permitted, but republication/redistribution requires IEEE permission.
See http://www.ieee.org/publications_standards/publications/rights/index.html for more information.

TABLE VII
POSITIONING PERFORMANCE OF DIFFERENT OBSTACLES

Obstacles	Method	Mean(m)	STD(m)	RMSE(m)
Human	Original	0.1584	0.1903	0.2474
	DTC-FCSVM	0.0567	0.1314	0.1430
	K-NN	0.1231	0.1539	0.1773
	LS-SVM	0.1035	0.1438	0.1807
Glass	Original	0.1733	0.2240	0.2830
	DTC-FCSVM	0.0619	0.0774	0.0991
	K-NN	0.1163	0.1615	0.1118
	LS-SVM	0.1224	0.1245	0.2029
Wall	Original	0.3366	0.3625	0.4944
	DTC-FCSVM	0.1116	0.1600	0.1950
	K-NN	0.1543	0.1959	0.2140
	LS-SVM	0.2579	0.2613	0.3017

VI. CONCLUSION

This paper proposed the UWB sensor positioning in three novel approaches. Firstly, three new novel CPPs is proposed to improve performance robustness in the classification of LOS and NLOS signal. Secondly, a DTC-FCSVM identification algorithm with higher utilization of parameter classification information including the proposed CCPs is proposed through the combination of threshold comparison and fuzzy credibility evaluation in SVM. Its Accuracy, Recall for LOS, and NLOS outperform the existing algorithms by at least 92.57 % in different scenarios. Finally, in the ranging error correction stage, the proposed approach leverages new CCPs to classify and correct the ranging error in both LOS and NLOS scenarios. The average errors for the corrected I-NLOS and I-LOS are less than 1m and 0.1 m respectively, resulting in more than 90 % of high-precision-ranging accuracy. Combined with the above NLOS/LOS identification and error correction, the system can improve the multi-scene dynamic positioning accuracy by 63.49 % with the mean error of about 0.1 m.

References

[1] F. L. Piccolo, "A new cooperative localization method for UMTS cellular networks", *Proc. IEEE Glob. Telecommun. Conf.*, pp. 1-5, 2008.

[2] M. Si, Y. Wang, C. K. Seow, H. Cao, H. Liu and L. Huang, "An Adaptive Weighted Wi-Fi FTM-Based Positioning Method in an NLOS Environment," *IEEE Sensors J.*, vol. 22, no. 1, pp. 472-480, 1 Jan.1, 2022.

[3] S. Xu, Y. Wang, M. Sun, M. Si, and H. Cao, "A Real-Time BLE/PDR Integrated System by Using an Improved Robust Filter for Indoor Position," *Applied Sciences*, vol. 11, no. 17, p. 8170, Sep. 2021.

[4] M. Sun, Y. Wang, S. Xu, H. Yang, and K. Zhang, "Indoor geomagnetic positioning using the enhanced genetic algorithm-based extreme learning machine," *IEEE Trans. Instrum. Meas.*, vol. 70, pp. 1–11, 2021.

[5] J. Khodjaev, Y. Park and J. Choi, "A novel UWB channel identification parameter for indoor positioning applications," *Ann. Telecommun.*, vol.66, no.9-10, pp. 501-506, Oct. 2011

[6] K. Yu, K. Wen, Y. Li, S. Zhang and K. Zhang, "A novel NLOS mitigation algorithm for UWB localization in harsh indoor environments," *IEEE Trans. Veh. Technol.*, vol. 68, no. 1, pp. 686-699, Jan. 2019.

[7] Q. L. Liang, "Radar sensor wireless channel modeling in foliage environment: UWB versus narrowband," *IEEE Sensors J.*, vol. 11, no. 6, pp. 1448–1457, Jun. 2011.

[8] J. Zhu and S. S. Kia, "Decentralized cooperative localization with LoS and NLoS UWB inter-agent ranging," *IEEE Sensors J.*, vol. 22, no. 6, pp. 5447-5456, Mar. 2021.

[9] X. Gan et al., "Doppler differential positioning technology using the BDS/GPS indoor array pseudolite system," *Sensors*, vol. 19, no. 20, pp. 4580, Oct. 2019.

[10] D. Coppens, A. Shahid, S. Lemey, B. Van Herbruggen, C. Marshall and E. De Poorter, "An Overview of UWB Standards and Organizations (IEEE 802.15.4, FiRa, Apple): Interoperability Aspects and Future Research Directions," in *IEEE Access*, vol. 10, pp. 70219-70241, 2022

[11] S. W. Chen, C. K. Seow, and S. Y. Tan, "Elliptical Lagrange-based NLOS tracking localization scheme," *IEEE Trans*. Wireless Commun., vol. 15, pp. 3212 – 3225, May 2016.

[12] *Decawave APS011 APPLICATION NOTE: Sources of error in TWR, Version 1.0.* Accessed: Sep. 4, 2019. [Online]. Available: https://www.decawave.com

[13] H. Zhang, S. Y. Tan and C. K. Seow, "TOA based indoor localization and tracking with inaccurate floor plan map via MRMSC-PHD filter," *IEEE Sensors J.*, vol. 19, no. 21, pp. 9869-9882, 2019.

[14] I. G ¨uvenc¸, C.-C. Chong, F. Watanabe, and H. Inamura, "NLOS identification and weighted least-squares localization for UWB systems using multipath channel statistics," *EURASIP J.* on Advances in Signal Processing, vol. 2008, pp. 1–14, 2008.

[15] X. Yang, "NLOS mitigation for UWB localization based on sparse pseudo-input Gaussian process," *IEEE Sensors J.*, vol. 18, no. 10, pp. 4311-4316, May 2018.

[16] J. Schroeder, S. Galler, K. Kyamakya, and K. Jobmann, "NLOS detection algorithms for ultra-wideband localization," in *Workshop on Positioning, Navigation and Commun. (WPNC)*, Mar. 2007 pp. 159– 166.

[17] J. Borras, P. Hatrack, and N. B. Mandayam, "Decision theoretic framework for NLOS identification," in *Proc. 48th Annual Int. Veh. Technol. Conf.*, vol. 2, Ottawa, Canada, May 1998, pp. 1583–1587.

[18] Z. Zeng, S. Liu, and L. Wang, "UWB/IMU integration approach with NLOS identification and mitigation," in *Proc. 52nd Annu. Conf. Inf. Sci. Syst. (CISS)*, Mar. 2018, pp. 1–6.

[19] Y. Jo, J. Lee, D. Ha, and S. Kang, "Accuracy enhancement for UWB indoor positioning using ray tracing," in *Proc. IEEE/ION Position. Loc. Navigat. Symp.*, 2006, pp. 565–568.

[20] D.-H. Kim and J.-Y. Pyun, "NLOS identification based UWB and PDR hybrid positioning system," *IEEE Access*, vol. 9, pp. 102917–102929, 2021

[21] A. Perttula, H. Leppäkoski, M. Kirkko-Jaakkola, P. Davidson, J. Collin and J. Takala, "Distributed indoor positioning system with inertial measurements and map matching," *IEEE Trans. Instrum. Meas.*, vol. 63, no. 11, pp. 2682-2695, Nov. 2014.

[22] B. Silva and G. P. Hancke, "IR-UWB-based non-line-of-sight identification in harsh environments: principles and challenges," *IEEE Trans. Ind. Informat.*, vol. 12, no. 3, pp. 1188–1195, Jun. 2016.

[23] I. Guvenc, C.-C. Chong, and F. Watanabe, "NLOS identification and mitigation for UWB localization systems," in Proc. *IEEE Wireless Commun. and Networking Conf.*, Kowloon, China, Mar. 2007, pp. 1571–1576.

[24] S. Venkatesh and R. M. Buehrer, "Non-line-of-sight identification in ultrawideband systems based on received signal statistics," *IET Microw. Antennas Propag.*, vol. 1, no. 6, pp. 1120–1130, Dec. 2007.

[25] S. Marano, W. M. Gifford, H. Wymeersch and M. Z. Win, "NLOS identification and mitigation for localization based on UWB experimental data," *IEEE J. Sel. Areas Commun.*, vol. 28, no. 7, pp. 1026-1035, Sep. 2010.

[26] H. Wymeersch, S. Marano, W. M. Gifford, and M. Z. Win, "A machine ` learning approach to ranging error mitigation for UWB localization," *IEEE Trans.* Commun., vol. 60, no. 6, pp. 1719–1728, Jun. 2012.

[27] R. Ying, T. Jiang and Z. Xing, "Classification of transmission environment in UWB communication using a support vector machine," *2012 IEEE Globecom Workshops*, 2012, pp. 1389-1393,

[28] C. Jiang, S. Chen, Y. Chen, D. Liu, and Y. Bo, "An UWB channel impulse response de-noising method for NLOS/LOS classification boosting," *IEEE Commun. Lett.*, vol. 24, no. 11, pp. 2513–2517, Nov. 2020.

[29] M. Kolakowski and J. Modelski, "Detection of direct path component absence in NLOS UWB channel," *2018 22nd International Microwave and Radar Conference (MIKON)*, 2018, pp. 247-250

[30] Q. Zhang, D. Zhao, S. Zuo, T. Zhang, and D. Ma, "A low complexity NLOS error mitigation method in UWB localization," in *Proc. IEEE Int. Conf. Commun.*, Shenzhen, China, Nov. 2015, pp. 1–5.

[31] F. Che *et al*., "Feature-Based Generalized Gaussian Distribution Method for NLoS Detection in Ultra-Wideband (UWB) Indoor Positioning System," in *IEEE Sensors Journal*, vol. 22, no. 19, pp. 18726-18739, 1 Oct.1, 2022

[32] F. Che, W. B. Abbas, Q. Z. Ahmed, B. Amjad, F. A. Khan and P. I. Lazaridis, "Weighted Naive Bayes Approach for Imbalanced Indoor Positioning System Using UWB," *2022 IEEE International Black Sea Conference on Communications and Networking (BlackSeaCom)*, 2022,

XXXX-XXXX © XXXX IEEE. Personal use is permitted, but republication/redistribution requires IEEE permission.
See http://www.ieee.org/publications_standards/publications/rights/index.html for more information.

pp. 72-76
[33] Z. Zeng, W. Yang, W. Wang, L. Wang and S. Liu, "Detection of the LOS/NLOS state change based on the CIR features," *Third World Conference on Smart Trends in Systems Security and Sustainablity (WorldS4)*, 2019, pp. 110-114
[34] M. Heidari, F. O. Akgul and K. Pahlavan, "Identification of the Absence of Direct Path in Indoor Localization Systems," *2007 IEEE 18th International Symposium on Personal, Indoor and Mobile Radio Communications*, 2007, pp. 1-6
[35] S. Wu, Y. Ma, Q. Zhang, and N. Zhang, "NLOS error mitigation for UWB ranging in dense multipath environments," in *Proc. IEEE Wireless Commun. and Networking Conf.*, Mar. 2007, pp. 1565–1570.
[36] X.-o. Song and X.-r. Wang, "An uwb cyclostationary detection algorithm based on nonparametric cusum," *International Conference on Innovative Mobile and Internet Services in Ubiquitous Computing*, pp. 94-103, 2020.
[37] F. Li, W. Xie, J. Wang, and S. Liu, "A new two-step ranging algorithm in NLOS environment for UWB systems," in *Proc. Asia-Pacific Conf. Commun.*, 2006, Art. no. 60572117.
[38] S. K. Rashid A. Saeed, "Ultra-wideband (UWB) geolocation in NLOS multipath fading environments," in *Proc. 13th IEEE Int. Conf. Netw. Jointly held with IEEE 7th Malaysia Int. Conf Communic*, Nov. 2005.
[39] P.-C. Chen, "A non-line-of-sight error mitigation algorithm in location estimation," in Proc. *IEEE Wireless Commun. Netw. Conf.*, Sep. 1999, vol. 1, pp. 316–320.
[40] L. Jiao, J. Xing, X. Zhang, J. Zhang and C. Zhao, "LCC-Rwgh: A NLOS Error Mitigation Algorithm for Localization in Wireless Sensor Network," *2007 IEEE International Conference on Control and Automation*, 2007, pp. 1354-1359
[41] W. Zhao, A. Goudar, and A. P. Schoellig, "Finding the right place: Sensor placement for uwb time difference of arrival localization in cluttered indoor environments," *IEEE Robotics and Automation Letters*, vol. 7, no. 3, pp. 6075–6082, 2022.
[42] L. Yao, Y.-W. A. Wu, L. Yao, and Z. Z. Liao, "An integrated IMU and UWB sensor based indoor positioning system," in Proc. Int. Conf. Indoor Positioning Indoor Navigat. (IPIN), Sapporo, Japan, 2017, pp. 1–8.
[43] Y. Huang, S. Mazuelas, F. Ge, and Y. Shen, "Indoor localization system with NLOS mitigation based on self-training," *IEEE Trans. Mobile Comput.*, early access, Feb. 4, 2022,
[44] G. J. Klir and B. Yuan, Fuzzy Sets and Fuzzy Logic: Theory and Applications, USA, NJ, Upper Saddle River:Prentice–Hall, 1995.
[45] L. Schmid, D. Salido-Monzu and A. Wieser, "Accuracy assessment and learned error mitigation of UWB ToF ranging," *Proc. Int. Conf. Indoor Positioning Indoor Navigat. (IPIN)*, pp. 1-8, Sep. 2019.
[46] M. J. Kuhn, J. Turnmire, M. R. Mahfouz, and A. E. Fathy, "Adaptive leading-edge detection in UWB indoor localization," in *Proc. IEEE Radio Wireless Symp.*, Jan. 2010, pp. 268–271.
[47] *DW1000 User Manual, Version 2.15.* Accessed: Sep. 4, 2019. [Online]. Available: https://www.decawave.com
[48] *DW1000 metrics for estimation of non line of sight operating conditions*, [online] Available: https://www.decawave.com.
[49] H. J. Zimmermann, *Fuzzy set theory–and its applications*, 4th ed. New York, NY, USA: Springer, 2001.
[50] E. Tóth-Laufer, "Improvement possibilities of the maximum defuzzification methods," in *2019 IEEE 23rd International Conference on Intelligent Engineering Systems (INES)*, 2019.
[51] H. Ma, L. Wang and B. Shen, "A new fuzzy support vector machines for class imbalance learning," *2011 International Conference on Electrical and Control Engineering*, 2011, pp. 3781-3784
[52] H. Yu, C. Sun, X. Yang, S. Zheng, and H. Zou, "Fuzzy support vector machine with relative density information for classifying imbalanced data," IEEE Trans. Fuzzy Syst., vol. 27, no. 12, pp. 2353–2367, Dec. 2019.
[53] P. Dai, Y. Yang, C. Zhang, X. Bao, H. Zhang, and Y. Zhang, "Analysis of target detection based on UWB NLOS ranging modeling," in *Proc. Ubiquitous Positioning, Indoor Navigat. Location-Based Services (UPINLBS)*, Wuhan, China, Mar. 2018, pp. 1–6
[54] L. Zhang, Y. Sun, Y. Su, J. Wang and Y. Li, "A Processing Approach for the NLOS error in UWB Ranging," *2021 IEEE 2nd International Conference on Big Data, Artificial Intelligence and Internet of Things Engineering (ICBAIE)*, 2021, pp. 518-526
[55] J. Ekstener, "Validation of Test Equipment for Active Safety," Dissertation, 2017.

XXXX-XXXX © XXXX IEEE. Personal use is permitted, but republication/redistribution requires IEEE permission.
See http://www.ieee.org/publications_standards/publications/rights/index.html for more information.